SEA96—A New Predictive Relation for Earthquake Ground Motions in Extensional Tectonic Regimes

P. Spudich, J.B. Fletcher, M. Hellweg, J. Boatwright, C. Sullivan, W.B. Joyner, T.C. Hanks, D.M. Boore, A. McGarr, L.M. Baker, and A.G. Lindh

U.S. Geological Survey

We present a new predictive relation for horizontal peak ground acceleration and 5% damped pseudo-velocity response spectrum appropriate for predicting earthquake ground motions in extensional tectonic regimes. This new empirical relation, which we denote "Sea96," was originally derived by Spudich et al. (1996) as part of a project to estimate seismic hazard at the site of a proposed nuclear waste repository at Yucca Mountain, Nevada. Because of the length and relative inaccessibility of that report, we are briefly presenting the Sea96 relation and its derivation here.

We developed our relation based on data from extensional regime earthquakes having moment magnitude $M >$ 5.0 recorded at distances less than 105 km. Extensional regions are regions in which the lithosphere is expanding areally. This areal expansion is the result of applied forces that yield a state of stress for which $S_v > S_{Hmax} > S_{Hmin}$, where S_v, S_{Hmax}, and S_{Hmin} represent principal stresses that are oriented approximately vertically and in two orthogonal horizontal directions. These terms are defined in McGarr and Gay (1978). Aside from obvious evidence of areal expansion, such as contemporary geodetic measurements and *in situ* stress measurements, extensional regimes usually present some or all of the following features: a mixture of normal-faulting and strike-slip earthquakes (we included earthquakes having both of these mechanisms in this study), recent volcanism, aligned volcanic features, lithospheric thinning, and high heat flow.

There are two reasons for restricting our attention to ground motion data from earthquakes in extensional provinces. First, there is observational evidence that the state of stress, extensional or compressional, affects the amplitude of the ground motion from an earthquake (McGarr, 1984; Abrahamson, 1993; Boore et al., 1994; Campbell and Bozorgnia, 1994). McGarr (1984) suggested that normal-faulting events have lower motions than strike-slip events. A second way in which the stress state might affect the recorded ground motion involves possible differences in wave propagation characteristics between extensional and compressional tectonic regimes. Extensional regimes have some degree of similarity in crustal structure worldwide. Christensen and Mooney (1995) report that extended crust and rifts have thinner crust and higher average crustal velocity gradients with depth than other continental crust. These factors might affect the geometric spreading of S waves, and they may affect the distances at which Moho reflections are observed. Mooney and Meissner (1992) state that in regions where the latest tectonic event was extensional, such as much of western Europe, the Basin and Range, and many passive margins, the lower crust tends to be highly reflective and the Moho tends to be nearly horizontal, generating readily observable Moho reflections.

Based on these considerations, the following groups of earthquakes were included in this study:

1. All earthquakes in Table 1 of Westaway and Smith (1989), by virtue of their normal-faulting mechanisms.
2. Earthquakes in Europe, New Zealand, and Central America if either their focal mechanisms or neotectonic stress indicators indicated extensional regime classification.
3. Earthquakes in Turkey occurring along extensional offsets in the Anatolian fault system.
4. Western United States events associated with active tectonic extension, such as those in the Basin and Range province, the Yellowstone hot spot, the Salton trough, and in volcanically or geothermally active areas like Long Valley, California.

All records used in this study were available digitally. We obtained the uncorrected digitized records from the data source and we sent them to a contractor (W. Silva, Pacific Engineering and Analysis) who performed the instrument correction and calculation of response spectra. For each response spectrum, we determined a passband in which the data were usable based on visual inspection of the Fourier amplitude spectra and the doubly-integrated displacements, and only data from within this band were used in the regression. We rejected records from structures of more than two

stories height, from deeply embedded basements, or from instruments that triggered during the S wave. For each earthquake we retained records recorded at distances greater than the "cutoff distance," the distance beyond the first untriggered accelerograph.

Recording sites were classified into two geologic catagories, rock and soil, following the classification scheme of Joyner and Boore (1981). We used the source-receiver distance metric of Joyner and Boore (1981, 1988), the shortest distance from the receiver to the vertical projection onto the Earth's surface of the fault rupture area. To determine this area, we first estimated the extent of the slipped region on the fault from ground motion inversions, geodetic inversions, aftershock distributions, or from a moment vs. rupture area relation (Wells and Coppersmith, 1994). The boundary of the rupture area was then taken to be a rectangular box enclosing this slipped region on the fault plane. Two earthquakes presented special cases. First, the 1979 Imperial Valley earthquake ruptured both the Imperial and Brawley Faults. For each station we chose the shorter of the distances to the two faults. Second, the 1980 Irpinia earthquake was a multiple event in which a large subevent occurred 40 s after the initiation of the main shock. Since the ground motions for the 40-s-subevent were well-separated from those of the earlier subevent, the two were treated as separate earthquakes. Table 1 shows the records used and their site geologies and distances.

We have developed new ground-motion prediction equations for geometric mean peak horizontal acceleration and 5 % damped response for the extensional region strong-motion data set. We initially attempted to derive a new regression relation solely from our extensional regime data set using the computer programs used by Boore *et al.* (1993), based on algorithms for the two-stage regression method described by Joyner and Boore (1993, 1994). For periods of 0.1 s and greater, the resulting relationship was satisfactory within the magnitude range covered by the extensional regime data set but was invalid when extrapolated to magnitudes 7.0 and larger. The main problem is that our extensional regime data set does not span a magnitude range that is wide enough to determine the coefficients of magnitude dependent terms accurately. Consequently, we were forced to discard our initial relationship.

In order to develop a relationship that would be valid for magnitude 7 and larger we adopted the magnitude dependence determined from a larger data set by Boore *et al.* (1993, 1994) and used our extensional regime data set to constrain the distance and site dependent terms. At each period we formed the following residuals,

$$r_i = y_i - b_2(M - 6) - b_3(M - 6)^2$$

where y_i is the common logarithm of the extensional regime data set ground-motion values, b_2 and b_3 are the Boore *et al.* (1994) coefficients, and M is moment magnitude. We then used the two-stage regression method (Joyner and Boore, 1993, 1994) to fit the residuals by an equation of the form

$$b_1 + b_5 \log_{10}(R) + b_6 \Gamma$$

where $R = \sqrt{r_{jb}^2 + h^2}$, r_{jb} is the Joyner-Boore distance, h is from Boore *et al.* (1994), Γ is 0 for rock sites and 1 for soil sites, and b_1, b_5, and b_6 are adjusted to fit the data. The resulting set of coefficients for 5% damped horizontal response was smoothed by fitting cubics or quadratics. Curves and calculated values for *psv* predicted from smoothed coefficients for a variety of magnitudes, distances, and site classes are given in Figure 1 and Table 2.

The equations for the predictive relations follow. The terms σ_1 and σ_2 are the standard deviations of ε_r and ε_e (Boore *et al.*, 1993, equation 1), which are respectively the record-to-record variation and the earthquake-to-earthquake variation in the residuals. Note that Table 3 contains a column for σ_3, which is the component standard deviation (*i.e.*, it is σ_c in Boore *et al.*, 1993, equation 3). The term σ_3 is not used to define the standard deviation of the geometric mean, but is used to form the standard deviation of the randomly oriented horizontal component, which is

$$\sqrt{\sigma_1^2 + \sigma_2^2 + \sigma_3^2} \ .$$

The resultant Sea96 relation may be used in the 5.0–7.7 magnitude range and the 0–70 km distance range for extensional regime earthquakes. Although data at distances greater than 70 km were used to develop Sea96, those data are few and they tend to be overpredicted by Sea96.

$$\log_{10} Y = b_1 + b_2(M - 6) + b_3(M - 6)^2 + b_4 R$$
$$+ b_5 \log_{10} R + b_6 \Gamma$$
$$\sigma_{\log Y} = \sqrt{\sigma_1^2 + \sigma_2^2}$$

where

$$R = \sqrt{r_{jb}^2 + h^2}$$

$$\Gamma = \begin{cases} 0 \text{ for rock} \\ 1 \text{ for soil} \end{cases}$$

$\sigma_{\log Y}$ = the standard deviation of $\log_{10} Y$

Y = peak horizontal acceleration (g) or pseudovelocity response (cm/s) at 5% damping for the geometric mean horizontal component of motion

Coefficients b_1, b_2, b_3, b_4, b_5, b_6, h, σ_1, and σ_2 are listed in Table 3 and can be downloaded from
http://agram.wr.usgs.gov/studies.html. ▨

TABLE 1
List of Records Used to Form the Regression Coefficients, with Site Geology and Distances.

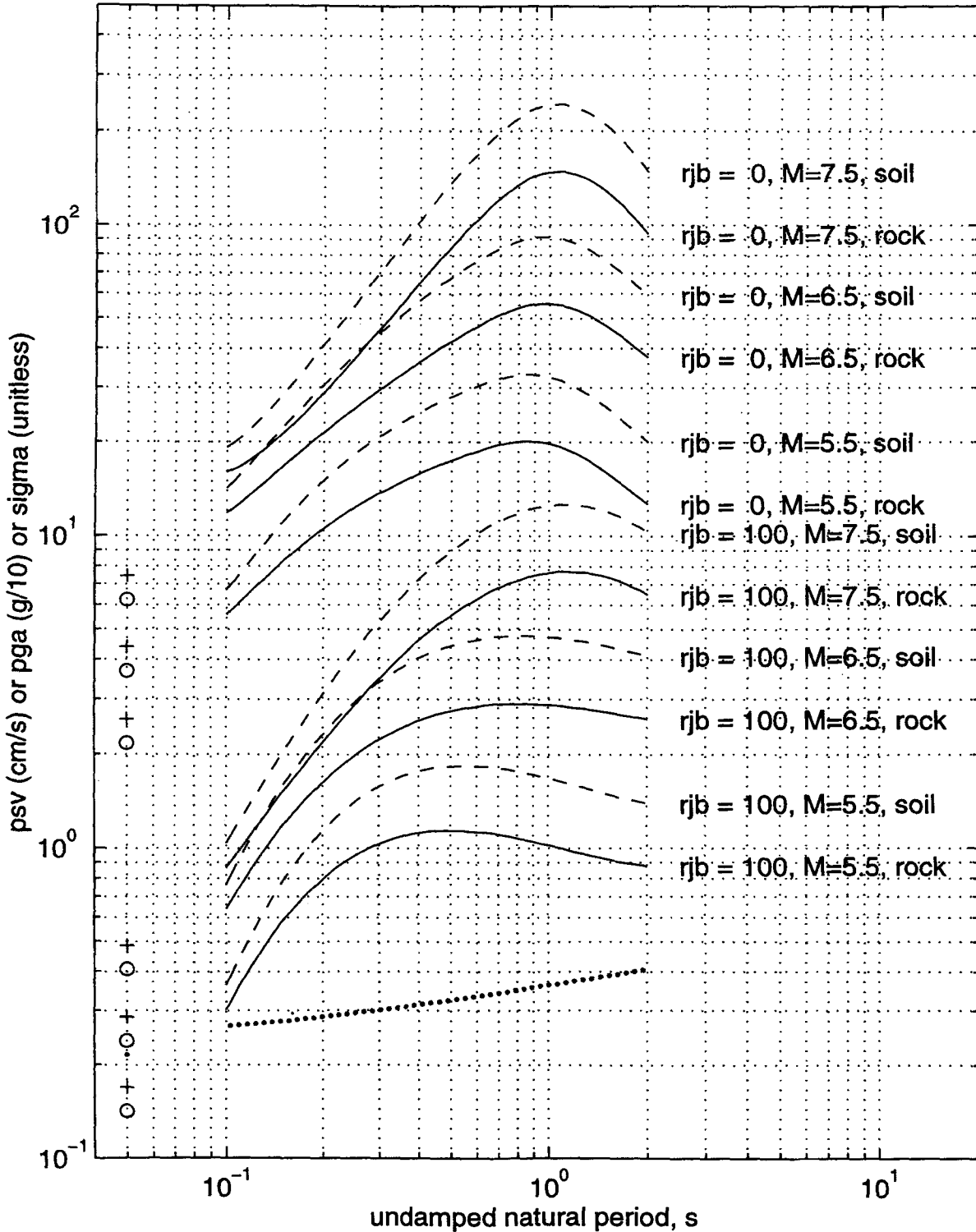| Date	Hr/Mn	Earthquake Name	M	Rake	Geol	r_{jb} (km)	Station Name
40.05.19	0536	Imperial Valley, CA	6.87	180	s	6.3	El Centro Array Sta. 9
72.12.23	0629	Managua, Nicaragua	6.20	−99	s	3.5	Managua: ESSO Refinery
79.09.19	2135	Valnerina, Italy	5.90	???	r	4.3	Cascia
79.09.19	2135	Valnerina, Italy	5.90	???	s	36.0	Bevagna
79.10.15	2316	Imperial Valley, CA	6.50	180	s	0.0	El Centro: Meloland Overpass
79.10.15	2316	Imperial Valley, CA	6.50	180	s	0.0	El Centro Array Sta. 6
79.10.15	2316	Imperial Valley, CA	6.50	180	s	0.0	Aeropuerto
79.10.15	2316	Imperial Valley, CA	6.50	180	s	0.0	Agrarias
79.10.15	2316	Imperial Valley, CA	6.50	180	s	0.4	Bonds Corner
79.10.15	2316	Imperial Valley, CA	6.50	180	s	0.6	El Centro Array Sta. 7
79.10.15	2316	Imperial Valley, CA	6.50	180	s	1.0	Cucapah
79.10.15	2316	Imperial Valley, CA	6.50	180	s	1.0	El Centro Array Sta. 5
79.10.15	2316	Imperial Valley, CA	6.50	180	s	3.9	El Centro Array Sta. 8
79.10.15	2316	Imperial Valley, CA	6.50	180	s	4.2	El Centro Array Sta. 4
79.10.15	2316	Imperial Valley, CA	6.50	180	s	5.2	El Centro: Differential Array
79.10.15	2316	Imperial Valley, CA	6.50	180	s	5.5	Holtville
79.10.15	2316	Imperial Valley, CA	6.50	180	s	7.2	Chihuahua
79.10.15	2316	Imperial Valley, CA	6.50	180	s	7.4	El Centro: Imp. Cnty Cntr FF
79.10.15	2316	Imperial Valley, CA	6.50	180	s	8.4	Brawley
79.10.15	2316	Imperial Valley, CA	6.50	180	s	8.6	El Centro Array Sta. 10
79.10.15	2316	Imperial Valley, CA	6.50	180	s	9.1	El Centro Array Sta. 3
79.10.15	2316	Imperial Valley, CA	6.50	180	s	10.4	Calexico
79.10.15	2316	Imperial Valley, CA	6.50	180	s	10.4	El Centro Array Sta. 2
79.10.15	2316	Imperial Valley, CA	6.50	180	s	12.5	El Centro Array Sta. 11
79.10.15	2316	Imperial Valley, CA	6.50	180	s	12.5	Parachute Test Site
79.10.15	2316	Imperial Valley, CA	6.50	180	s	13.5	Compuertas
79.10.15	2316	Imperial Valley, CA	6.50	180	s	14.6	Westmorland
79.10.15	2316	Imperial Valley, CA	6.50	180	r	15.2	Cerro Prieto
79.10.15	2316	Imperial Valley, CA	6.50	180	s	15.9	El Centro Array Sta. 1
79.10.15	2316	Imperial Valley, CA	6.50	180	s	18.0	El Centro Array Sta. 12
79.10.15	2316	Imperial Valley, CA	6.50	180	s	21.9	Delta
79.10.15	2316	Imperial Valley, CA	6.50	180	s	22.0	El Centro Array Sta. 13
79.10.15	2316	Imperial Valley, CA	6.50	180	s	23.3	Calipatria
79.10.15	2316	Imperial Valley, CA	6.50	180	r	24.5	Superstition Mtn.
79.10.15	2316	Imperial Valley, CA	6.50	180	s	31.8	Victoria
79.10.15	2316	Imperial Valley, CA	6.50	180	s	35.4	Niland
79.10.15	2316	Imperial Valley, CA	6.50	180	s	48.8	Coachella Canal Sta. 4
80.05.25	1633	Mammoth Lakes, CA	6.20	−35	s	1.1	Convict Creek
80.05.25	1633	Mammoth Lakes, CA	6.20	−35	s	4.5	Mammoth Lakes H.S.
80.05.25	1649	Mammoth Lakes, CA	5.80	0	s	2.9	Convict Creek
80.05.25	1649	Mammoth Lakes, CA	5.80	0	s	3.5	Mammoth Lakes H.S.
80.05.25	1944	Mammoth Lakes, CA	5.80	−11	s	1.7	Convict Creek
80.05.25	1944	Mammoth Lakes, CA	5.80	−11	r	10.1	Long Valley Dam

TABLE 1 (Continued)
List of Records Used to Form the Regression Coefficients, with Site Geology and Distances.

Date	Hr/Mn	Earthquake Name	M	Rake	Geol	r_{jb} (km)	Station Name
80.05.25	2035	Mammoth Lakes, CA	5.70	???	s	2.8	Convict Creek
80.05.25	2035	Mammoth Lakes, CA	5.70	???	r	14.2	Long Valley Dam
80.05.27	1450	Mammoth Lakes, CA	6.00	−28	s	5.9	Convict Creek
80.05.27	1450	Mammoth Lakes, CA	6.00	−28	s	6.0	Fish and Game
80.05.27	1450	Mammoth Lakes, CA	6.00	−28	s	41.0	Bishop—LADWP
80.05.27	1450	Mammoth Lakes, CA	6.00	−28	s	41.8	Benton
80.06.09	0328	Victoria, Mexico	6.32	0	s	25.1	Cucapah
80.06.09	0328	Victoria, Mexico	6.32	0	s	38.6	Mexicali SAHOP
80.11.23	1834	Irpinia, Italy	6.90	−90	r	10.9	Bagnoli Irpinio
80.11.23	1834	Irpinia, Italy	6.90	−90	r	11.2	Calitri
80.11.23	1834	Irpinia, Italy	6.90	−90	r	16.2	Sturno
80.11.23	1834	Irpinia, Italy	6.90	−90	r	24.9	Bisaccia
80.11.23	1834	Irpinia, Italy	6.90	−90	r	25.9	Rionero in Vulture
80.11.23	1834	Irpinia, Italy	6.90	−90	s	36.3	Mercato San Severino
80.11.23	1834	Irpinia, Italy	6.90	−90	s	43.1	Bovino
80.11.23	1834	Irpinia, Italy	6.90	−90	r	63.0	Arienzo
80.11.23	1834	Irpinia, Italy	6.90	−90	r	67.7	Torre del Greco
80.11.23	1835	Irpinia AS, Italy	6.20	−90	r	8.4	Calitri
80.11.23	1835	Irpinia AS, Italy	6.20	−90	r	18.2	Bagnoli Irpinio
80.11.23	1835	Irpinia AS, Italy	6.20	−90	r	20.3	Sturno
80.11.23	1835	Irpinia AS, Italy	6.20	−90	r	22.1	Bisaccia
80.11.23	1835	Irpinia AS, Italy	6.20	−90	r	22.3	Rionero in Vulture
80.11.23	1835	Irpinia AS, Italy	6.20	−90	r	28.9	Auletta
80.11.23	1835	Irpinia AS, Italy	6.20	−90	s	41.9	Brienza
80.11.23	1835	Irpinia AS, Italy	6.20	−90	s	43.0	Bovino
80.11.23	1835	Irpinia AS, Italy	6.20	−90	s	43.9	Mercato San Severino
80.11.23	1835	Irpinia AS, Italy	6.20	−90	s	64.4	Tricarico
81.04.26	1209	Westmorland, CA	5.90	0	s	6.2	Westmorland
81.04.26	1209	Westmorland, CA	5.90	0	s	8.0	Salton Sea Wildlife Refuge
81.04.26	1209	Westmorland, CA	5.90	0	s	15.1	Niland
81.04.26	1209	Westmorland, CA	5.90	0	s	15.3	Brawley
81.04.26	1209	Westmorland, CA	5.90	0	s	16.5	Parachute Test Site
81.04.26	1209	Westmorland, CA	5.90	0	r	19.1	Superstition Mtn.
83.08.06	1543	N. Aegean Sea, Greece	6.74	−179	s	81.0	Ierissos
83.10.28	1406	Borah Peak, ID	6.90	−70	s	82.7	CPP—601—basement
83.10.28	1406	Borah Peak, ID	6.90	−70	s	84.9	TAN—719
83.10.29	2329	Borah Peak AS, ID	5.10	−65	s	16.9	BOR
83.10.29	2329	Borah Peak AS, ID	5.10	−65	r	22.0	CEM
83.10.29	2329	Borah Peak AS, ID	5.10	−65	r	49.3	HAU
84.05.07	1749	Lazio—Abruzzo, Italy	5.80	−96	r	19.2	Atina
84.05.07	1749	Lazio—Abruzzo, Italy	5.80	−96	s	30.2	Pontecorvo
84.05.07	1749	Lazio—Abruzzo, Italy	5.80	−96	s	41.0	Isernia—San'agapito
84.05.07	1749	Lazio—Abruzzo, Italy	5.80	−96	s	45.6	Roccamonfina

TABLE 1 (Continued)
List of Records Used to Form the Regression Coefficients, with Site Geology and Distances.

Date	Hr/Mn	Earthquake Name	M	Rake	Geol	r_{jb} (km)	Station Name
84.05.07	1749	Lazio—Abruzzo, Italy	5.80	−96	s	49.7	Garigliano—Centrale Nucleare
86.07.20	1429	Chalfant Valley FS, CA	5.80	20	s	7.4	Chalfant
86.07.20	1429	Chalfant Valley FS, CA	5.80	20	r	14.0	Bishop—Paradise Lodge
86.07.20	1429	Chalfant Valley FS, CA	5.80	20	s	17.5	Bishop—LADWP
86.07.20	1429	Chalfant Valley FS, CA	5.80	20	s	25.0	Benton
86.07.20	1429	Chalfant Valley FS, CA	5.80	20	s	25.2	Crowley Lake
86.07.21	1442	Chalfant Valley, CA	6.30	−160	s	4.4	Chalfant
86.07.21	1442	Chalfant Valley, CA	6.30	−160	r	17.9	Bishop—Paradise Lodge
86.07.21	1442	Chalfant Valley, CA	6.30	−160	s	19.4	Bishop—LADWP
86.07.21	1442	Chalfant Valley, CA	6.30	−160	s	20.3	Benton
86.07.21	1442	Chalfant Valley, CA	6.30	−160	r	21.0	Long Valley Dam
86.07.21	1442	Chalfant Valley, CA	6.30	−160	s	24.7	Crowley Lake
86.07.21	1442	Chalfant Valley, CA	6.30	−160	s	28.7	McGee Creek
86.07.21	1442	Chalfant Valley, CA	6.30	−160	s	31.8	Convict Creek
86.07.21	1442	Chalfant Valley, CA	6.30	−160	r	37.2	Mammoth Lakes Sheriff Subst.
86.07.21	1442	Chalfant Valley, CA	6.30	−160	r	56.8	Tinemaha Reservoir—FF
86.07.21	1451	Chalfant Valley AS, CA	5.60	???	r	11.9	Bishop—Paradise Lodge
86.07.21	1451	Chalfant Valley AS, CA	5.60	???	s	15.2	Chalfant
86.07.21	1451	Chalfant Valley AS, CA	5.60	???	s	24.9	Bishop—LADWP
86.07.31	0722	Chalfant Valley AS, CA	5.80	160	s	8.7	Chalfant
86.07.31	0722	Chalfant Valley AS, CA	5.80	160	s	22.1	Bishop—LADWP
86.10.10	1749	San Salvador	5.76	0	s	2.1	CIG, San Salvador
86.10.10	1749	San Salvador	5.76	0	s	3.7	IGN, San Salvador
87.03.02	0142	Edgecumbe MS, NZ	6.60	−110	s	18.9	Matahina Dam
87.03.02	0142	Edgecumbe MS, NZ	6.60	−110	s	70.1	Maraenui ES
87.03.02	0150	Edgecumbe AS, NZ	5.80	???	s	33.6	Matahina Dam
87.11.24	0154	Elmore Ranch, CA	6.20	180	s	19.8	Imperial Wildlife
87.11.24	1315	Superstition Hills, CA	6.60	178	s	13.1	Westmorland
87.11.24	1315	Superstition Hills, CA	6.60	178	s	18.2	El Centro: Imp. Cnty Cntr FF
92.03.13	1718	Erzincan, Turkey	6.70	−163	s	1.8	Erzincan
92.04.13	0120	Roermond, Netherl.	5.31	−94	r	55.8	GSH
92.04.13	0120	Roermond, Netherl.	5.31	−94	r	80.7	OLF
92.04.13	0120	Roermond, Netherl.	5.31	−94	r	102.1	WBS
92.06.29	1014	Little Skull Mt., NV	5.70	−70	s	14.1	Lathrop—A
92.06.29	1014	Little Skull Mt., NV	5.70	−70	r	23.8	NTS C.P.1 A
92.06.29	1014	Little Skull Mt., NV	5.70	−70	r	45.2	Beatty
92.06.29	1014	Little Skull Mt., NV	5.70	−70	s	58.6	Pahrump 2
92.06.29	1014	Little Skull Mt., NV	5.70	−70	s	63.7	Pahrump 1
92.06.29	1014	Little Skull Mt., NV	5.70	−70	r	98.2	Scottie's Castle
92.06.29	1014	Little Skull Mt., NV	5.70	−70	s	98.9	Ann Road
92.06.29	1014	Little Skull Mt., NV	5.70	−70	r	99.4	Calico Basin
94.09.12	1223	Double Spring Flat, NV	5.90	−25	s	12.5	Woodfords

▲ Figure 1. Ground motions and sigma predicted by Sea96 for distances of 0 and 100 km, magnitudes 5.5, 6.5, and 7.5, and for rock and soil conditions. The 5% damped geometric mean horizontal pseudo-velocity responses are for rock (solid lines) and soil (dashed lines). Geometric mean peak horizontal acceleration, multiplied by a factor of 10, plotted at 0.05 s period for rock sites (circles) and soil sites (plus signs). Dispersion $\sigma_{\log Y}$ (dotted line) shown as function of period.

TABLE 2.
Predicted pga, psv, and sigma for Sea96 evaluated numerically for selected magnitudes, distances, periods, and site conditions

M	r_{jb} (km)	site	pga	0.1 s	0.5 s	2.0 s
5.5	0	r	2.1710×10^{-1}	5.5728	1.7433×10^{1}	1.2651×10^{1}
5.5	0	s	2.5922×10^{-1}	6.6845	2.8014×10^{1}	2.0050×10^{1}
5.5	100	r	1.4154×10^{-2}	3.0276×10^{-1}	1.1348	8.7610×10^{-1}
5.5	100	s	1.6899×10^{-2}	3.6317×10^{-1}	1.8236	1.3885
6.5	0	r	3.6785×10^{-1}	1.1832×10^{1}	4.2207×10^{1}	3.7422×10^{1}
6.5	0	s	4.3920×10^{-1}	1.4193×10^{1}	6.7824×10^{1}	5.9309×10^{1}
6.5	100	r	2.3981×10^{-2}	6.4284×10^{-1}	2.7475	2.5915
6.5	100	s	2.8633×10^{-2}	7.7109×10^{-1}	4.4150	4.1073
7.5	0	r	6.2326×10^{-1}	1.5998×10^{1}	8.5385×10^{1}	9.3352×10^{1}
7.5	0	s	7.4416×10^{-1}	1.9190×10^{1}	1.3721×10^{2}	1.4795×10^{2}
7.5	100	r	4.0632×10^{-2}	8.6917×10^{-1}	5.5582	6.4648
7.5	100	s	4.8514×10^{-2}	1.0426	8.9317	1.0246×10^{1}
$\sigma_{\log Y}$			2.1600×10^{-1}	2.6800×10^{-1}	3.2343×10^{-1}	4.0746×10^{-1}

TABLE 3.
Smoothed coefficients for regression relation Sea96, for geometric mean horizontal pga and 5% damped psv

$T(s)$	NR	NQ	b_1	b_2	b_3	b_4	b_5	b_6	h (km)	σ_1	σ_2	σ_3
pga	128	30	0.156	0.229	0.000	0.0	−0.945	0.077	5.57	0.216	0.000	0.094
0.100	118	29	1.772	0.327	−0.098	0.0	−1.051	0.079	6.27	0.268	0.000	0.111
0.110	118	29	1.830	0.318	−0.100	0.0	−1.043	0.092	6.65	0.270	0.000	0.112
0.120	118	29	1.876	0.313	−0.101	0.0	−1.035	0.102	6.91	0.272	0.000	0.114
0.130	118	29	1.912	0.309	−0.101	0.0	−1.026	0.112	7.08	0.274	0.000	0.115
0.140	118	29	1.941	0.307	−0.100	0.0	−1.018	0.120	7.18	0.276	0.000	0.116
0.150	118	29	1.964	0.305	−0.099	0.0	−1.009	0.127	7.23	0.277	0.001	0.117
0.160	118	29	1.982	0.305	−0.098	0.0	−1.001	0.134	7.24	0.279	0.003	0.118
0.170	118	29	1.996	0.305	−0.096	0.0	−0.994	0.139	7.21	0.281	0.005	0.119
0.180	118	29	2.008	0.306	−0.094	0.0	−0.986	0.145	7.16	0.283	0.008	0.120
0.190	118	29	2.016	0.308	−0.092	0.0	−0.979	0.150	7.10	0.284	0.010	0.120
0.200	118	29	2.023	0.309	−0.090	0.0	−0.972	0.154	7.02	0.286	0.012	0.121
0.220	118	29	2.032	0.313	−0.086	0.0	−0.958	0.162	6.83	0.289	0.015	0.122
0.240	118	29	2.035	0.318	−0.082	0.0	−0.946	0.168	6.62	0.292	0.019	0.124
0.260	118	29	2.036	0.323	−0.078	0.0	−0.935	0.174	6.39	0.295	0.022	0.125
0.280	118	29	2.034	0.329	−0.073	0.0	−0.925	0.179	6.17	0.297	0.024	0.126
0.300	118	29	2.030	0.334	−0.070	0.0	−0.915	0.183	5.94	0.300	0.027	0.126
0.320	118	29	2.025	0.340	−0.066	0.0	−0.907	0.187	5.72	0.302	0.030	0.127
0.340	118	29	2.020	0.345	−0.062	0.0	−0.899	0.190	5.50	0.304	0.032	0.128
0.360	118	29	2.014	0.350	−0.059	0.0	−0.892	0.193	5.30	0.307	0.034	0.128
0.380	118	29	2.008	0.356	−0.055	0.0	−0.885	0.196	5.10	0.309	0.036	0.129
0.400	118	29	2.001	0.361	−0.052	0.0	−0.879	0.198	4.91	0.311	0.038	0.129

TABLE 3. (continued)
Smoothed coefficients for regression relation Sea96, for geometric mean horizontal *pga* and 5% damped *psv*

$T(s)$	NR	NQ	b_1	b_2	b_3	b_4	b_5	b_6	h (km)	σ_1	σ_2	σ_3
0.420	118	29	1.995	0.365	−0.049	0.0	−0.874	0.200	4.74	0.313	0.040	0.130
0.440	118	29	1.989	0.370	−0.047	0.0	−0.869	0.202	4.57	0.315	0.042	0.130
0.460	118	29	1.983	0.375	−0.044	0.0	−0.864	0.203	4.41	0.317	0.043	0.131
0.480	118	29	1.977	0.379	−0.042	0.0	−0.860	0.205	4.26	0.319	0.045	0.131
0.500	118	29	1.971	0.384	−0.039	0.0	−0.857	0.206	4.13	0.320	0.047	0.132
0.550	118	29	1.958	0.394	−0.034	0.0	−0.849	0.209	3.82	0.325	0.050	0.132
0.600	118	29	1.946	0.403	−0.030	0.0	−0.843	0.211	3.57	0.329	0.054	0.133
0.650	118	29	1.937	0.411	−0.026	0.0	−0.838	0.212	3.36	0.332	0.057	0.134
0.700	118	29	1.929	0.418	−0.023	0.0	−0.835	0.213	3.20	0.336	0.059	0.134
0.750	118	29	1.922	0.425	−0.020	0.0	−0.833	0.214	3.07	0.339	0.062	0.135
0.800	118	29	1.917	0.431	−0.018	0.0	−0.833	0.214	2.98	0.343	0.065	0.135
0.850	118	29	1.914	0.437	−0.016	0.0	−0.833	0.215	2.92	0.346	0.067	0.136
0.900	118	29	1.912	0.442	−0.015	0.0	−0.833	0.215	2.89	0.349	0.069	0.136
0.950	118	29	1.911	0.446	−0.014	0.0	−0.835	0.215	2.88	0.352	0.071	0.136
1.000	118	29	1.912	0.450	−0.014	0.0	−0.837	0.214	2.90	0.354	0.073	0.137
1.100	109	27	1.916	0.457	−0.013	0.0	−0.842	0.214	2.99	0.359	0.077	0.137
1.200	108	27	1.923	0.462	−0.014	0.0	−0.850	0.213	3.14	0.364	0.080	0.138
1.300	108	27	1.934	0.466	−0.015	0.0	−0.858	0.212	3.36	0.369	0.083	0.138
1.400	107	27	1.948	0.469	−0.017	0.0	−0.868	0.210	3.62	0.373	0.086	0.138
1.500	107	27	1.964	0.471	−0.019	0.0	−0.879	0.209	3.92	0.377	0.089	0.139
1.600	107	27	1.981	0.472	−0.022	0.0	−0.890	0.207	4.26	0.381	0.091	0.139
1.700	99	27	2.001	0.473	−0.025	0.0	−0.902	0.205	4.62	0.385	0.093	0.139
1.800	99	27	2.022	0.472	−0.029	0.0	−0.914	0.204	5.01	0.388	0.096	0.139
1.900	99	27	2.045	0.472	−0.032	0.0	−0.927	0.202	5.42	0.392	0.098	0.139
2.000	99	27	2.068	0.471	−0.037	0.0	−0.940	0.200	5.85	0.395	0.100	0.140

ACKNOWLEDGMENTS

REFERENCES

Abrahamson, N.A. (1993). Estimation of hanging wall and foot wall effects on strong ground motions (to appear in *Proc. International Workshop on Strong Ground Motion*, Menlo Park, CA, December 13–17, 1993).

Boore, D.M., W.B. Joyner, and T.E. Fumal (1993). Estimation of response spectra and peak accelerations from western North American earthquakes: An interim report, *U.S. Geol. Surv. Open-File Rep. 93-509*, 72 pp.

Boore, D.M., W.B. Joyner, and T.E. Fumal (1994). Estimation of response spectra and peak accelerations from western North American earthquakes: An interim report, Part 2, *U.S. Geol. Surv. Open-File Rep. 94-127*, 40 pp.

Campbell, K.W. and Y. Bozorgnia (1994). Near-source attenuation of peak horizontal acceleration from Worldwide Accelerograms recorded from 1957 to 1993, *Fifth U.S. Nat'l Conf. on Eq. Eng.*, Chicago, IL, July 10–14, 1994.

Christensen, N. and W.D. Mooney (1995). Seismic velocity structure and composition of the continental crust: a global view, *J. Geophys. Res.*, **100**, 9,761–9,788.

Joyner, W.B., and D.M. Boore (1981). Peak horizontal acceleration and velocity from strong motion records including records from the 1979 Imperial Valley, California, earthquake, *Bull. Seism. Soc. Am.*, **71**, 2,011–2,038.

Joyner, W.B., and D.M. Boore (1982). Prediction of earthquake response spectra, *U.S. Geol. Surv. Open-File Rep. 82–977*, 16 pp.

Joyner, W.B., and D.M. Boore (1988). Measurement, characterization, and prediction of strong ground motion, *Proc. Earthq. Eng. Soil Dynamics II*, GT Div/ASCE, Park City, UT, June 27–30, 1988.

Joyner, W.B., and D.M. Boore (1993). Methods for regression analysis of strong motion data, *Bull. Seism. Soc. Am.*, **83**, 469–487.

Joyner, W.B., and D.M. Boore, 1994, Errata—Methods for regression analysis of strong motion data, *Bull. Seism. Soc. Am.*, **84**, 955–956.

McGarr, A. (1984). Scaling of ground motion parameters, state of stress, and focal depth, *J. Geophys. Res.*, **89**, 6,969–6,979.

McGarr, A. and N.C. Gay (1978). State of stress in the earth's crust, *Ann. Rev. Earth and Plan. Sci.*, **6**, 405–436.

Mooney, W.D. and R. Meissner (1992)., Multi-genetic origin of crustal reflectivity: a review of seismic reflection profiling of the continental lower crust and Moho, in *The Lower Continental Crust*, eds. D. M. Fountain, R. Arculus, and R. W. Kay, Elsevier, Amsterdam, pp. 45–79.

Spudich, P., J. Fletcher, M. Hellweg, J. Boatwright, C. Sullivan, W. Joyner, T. Hanks, D. Boore, A. McGarr, L. Baker, and A. Lindh (1996). Earthquake ground motions in extensional tectonic regimes, *U.S. Geological Survey Open File Report 96-292*, 351 pp.

Westaway, R. and R.B. Smith (1989). Strong ground motion in normal-faulting earthquakes, *Geophys. J.*, **96**, 529–559.

Wells, D.L. and K.J. Coppersmith (1994). New empirical relationships among magnitude, rupture length, rupture width, rupture area, and surface displacement, *Bull. Seism. Soc. Am.*, **84**, 974–1,002.

U.S. Geological Survey
Western Earthquake Hazards Team
Seismology Section
Mail Stop 977
345 Middlefield Road
Menlo Park, CA 94025